

Fundamental aspects and applications of electrodeposited nanostructured metals*

Pietro L. Cavallotti[‡], Luca Nobili, Silvia Franz, and Antonello Vicenzo

Department of Chemistry, Materials and Chemical Engineering “Giulio Natta”, Polytechnic University of Milan, Via Mancinelli 7, 20131 Milan, Italy

Abstract: A rational understanding of what occurs during electrocrystallization, defined at a nanolevel, is developed to control electrodeposition processes. The electrokinetic behavior of the elements in solutions and the electrodeposits structure resulting from the electron exchange reaction at the cathodic surface are taken into consideration and compared. Transient electrokinetic parameters are measured with the secondary current pulse (SCP) technique, where a square galvanostatic pulse of a few ms duration is superimposed on the cathode while electrodeposition is running. Two parameters are obtained, the transient Tafel slope and the adsorption pseudo-capacitance; whilst a third parameter, the diffusive time constant, must be introduced if the overvoltage does not arrive to a steady state during the short pulse period. These parameters are related to the growth of different structures and permit a good control of the process. Control of the growth with nanodefinition is key to the development of innovative processes to keep pace with more and more demanding applications and environmental challenges. Examples are given to stress the relevance of the theoretical framework and to show possible implications for electrodeposition technology and its applications.

Keywords: cobalt; electrochemical kinetics; electrodeposition; nanostructures; nickel–cobalt.

INTRODUCTION

Electrocrystallization can be rationally interpreted if we take into consideration and compare the electrokinetic behavior of the elements and the electrodeposits structure, resulting from the electron exchange reaction at the cathodic surface. The macroscopic quantities, statistically mediated, which can describe the electrochemical behavior, depend on the force fields acting at the atomic level, with quantum-mechanical rules; it is thus possible to find relations between the electrochemical parameters, in steady state and in transient conditions, and the structure morphology and crystallography.

The interpretation of electrodeposits crystal growth underlines some important characteristics that can be only briefly mentioned here. The foundation and early development of electrocrystallization studies had mainly a phenomenological character, as can be argued re-examining the work of Finch's school [1–6], which particularly emphasized the role of lateral or outward growth on the electrodeposits structure, and the fundamental contribution of Fischer. In his work [7–12], Fischer developed an articulated, interpretative frame relating deposits microstructure and the type and degree of surface inhibition, recognizing five main growth types for polycrystalline electrodeposits: field-oriented isolated;

*Paper based on a presentation made at the 2nd Regional Symposium on Electrochemistry: South East Europe (RSE SEE-2), Belgrade, Serbia, 6–10 June 2010. Other presentations are published in this issue, pp. 253–358.

[‡]Corresponding author

basis-oriented reproduction; twinning intermediate; field-oriented texture; unoriented dispersion type, a model later revisited and refined in some respects in the work of Winand [13].

In that context, a much debated and investigated aspect of electrodeposits growth structure was the development of texture. In fact, an early attempt to force into a theoretical framework the phenomenological landscape emerging from electrocrystallization studies addressed this very aspect. This was the objective pursued by Pangarov [14–16], who extended the Kossel and Stranski model of two-dimensional nucleation and monatomic layer growth to electrodeposition, stressing the importance of the energetics of crystal formation on the development of texture. The legacy of Fischer, i.e., the concept of surface inhibition as growth determining factor in electrodeposition, had as well a definite strong impact in this direction. Texture formation in nickel electrodeposition was the playground where the model was tested, first by Reddy [17,18] who attributed a fundamental role to inhibition due to hydrogen presence at the surface and later on by Froment and Spyrellis schools [19–34], who attributed the observed structures to different types of inhibition—by hydrogen (molecular or atomic), hydroxides, or organics—and showed the different crystallographic features of these textures, [211] and [110] presenting perpendicular twins and [100] with no features attributed to a free mode of growth.

Against this briefly sketched historical background, fundamental studies in metal electrocrystallization have evolved in recent years along new and diverse directions, exploring nucleation and growth phenomena over wide time and length scales [35]. The interest in this research area has been enhanced by the implementation of electrodeposition processes in key technology applications [36–38] and backed up by the availability of in situ imaging and spectroscopic and chemical probing techniques. This renewed experimental activity has been paralleled by theoretical development stemming from the elaboration of an already established theoretical framework, in particular, the atomistic theory of nucleation [39], or, alternatively, from previously unexplored theoretical approaches, such as kinetic Monte Carlo simulation of crystal growth and texture formation in electrodeposits [40,41]. All these developments are now converging in a highly interdisciplinary and fascinating research area with strong relevance to the exploding field of nanotechnology [42].

Notwithstanding the great advances that have been made in the field of electrocrystallization, major issues remain open and the exploitation of research results is challenged by the complexity of electrodeposition processes and the variety of its applications. In this respect, the investigation of the relationship between fundamental macroscopic properties, characterizing growth process and crystal structure, has been a viable approach to unify the phenomenological landscape and define a general frame for discussing the link bridging kinetics and structure in electrocrystallization.

Piontelli [43–45] introduced a classification of the electrokinetic behavior of elements in aqueous solutions [46], based on their ionic and lattice properties, with reference to a Born–Haber cycle. He classified the metals as electrokinetically *normal*, *intermediate*, or *inert*. Normal metals show very low metal ion discharge overvoltage (in other words, high metal ion exchange current density i_M°), and high hydrogen overvoltage (low i_H°). Inert metals strongly interact with the solvent water with very high metal ion discharge overvoltage (low i_M°) and low hydrogen overvoltage (high i_H°). Within this frame, it was also possible to follow the electrodeposition of metals on single-crystal surfaces [47,48], proposing a general relation between electrokinetic behavior and growth in electrodeposition.

In this paper, we will extend Piontelli's classification, making reference to the normality–inertia parameter [49,50], and propose an interpretation of the growth mode of metals electrodeposited from simple solutions, comparing the structures and textures obtained with the electrolyte electrokinetic behavior.

THE NORMALITY–INERTIA PARAMETER

Ionic and lattice properties of the elements determine electrochemical kinetics and structure of deposits; by means of a Born–Haber cycle, it is possible to relate the enthalpy change for the metal exchange reaction to other fundamental physical quantities, such as atomization, ionization, and hydration

enthalpies [51,52]. We refer to an ideal galvanic chain $M/\epsilon_M \parallel \epsilon_H/\text{SHE}$ of metallic and electrolytic conductors in series, homogeneous, with the only exception of the interphase regions of atomic dimension, with contact phases at equilibrium, chemical modifications arising only from the current circulation, and the electromagnetic field not influenced by distribution of true charges, where one part is the electroic element and the other the reference standard hydrogen electrode (SHE).

The cell chemical reaction is



The electromotive force for the cell reaction is

$$E^\circ = \frac{-\Delta h_{\text{at}}^\circ - \Delta h_{\text{ion}}^\circ - \Delta h_{\text{hydr}}^\circ + T \Delta s_{\text{cell}}^\circ}{zF} + K_{\text{SHE}} \quad (2)$$

where the cell enthalpy change is given by means of the three contribution to the Born–Haber cycle.

The normal hydrogen electrode constant K_{SHE} is determined from the enthalpy changes for H_2 discharge, $\Delta h_{\text{atH}^+}^\circ = 2.2594$ V, $\Delta h_{\text{ionH}^+}^\circ = 13.6626$ V and $\Delta h_{\text{hydrH}^+}^\circ = -11.3075$ V, where the value determined by Halliwell and Nyburg [53] is attributed to the H^+ hydration enthalpy and the values reported by Dasent [54], Latimer [55], and Bard, Parsons, and Jordan [56] to the other enthalpy changes. Thus, we obtain: $K_{\text{SHE}} = 4.6142$ V.

The cell enthalpy change, expressed in volts and with reference to SHE, becomes

$$\frac{\Delta h_{\text{cell}}^\circ (M_{\text{aq}}^{z+})}{zF} = \frac{\Delta h_{\text{at}}^\circ + \Delta h_{\text{ion}}^\circ + \Delta h_{\text{hydr}}^\circ}{zF} - 4.61421 \quad (3)$$

From the given quantities [53–55] and from calculated values of the entropy change (from the isothermal temperature coefficients dE°/dT_{is} [57]), when known, or estimated values in the Latimer approximation [55], we obtain the results in Table 1, which show a very good approximation of the experimental E° values. The atomization enthalpy change is related to the melting temperature of the element; ionization and hydration enthalpy changes have high absolute values with opposite signs, increasing with the ion valence; their difference is of the same order of the atomization term.

Table 1 Standard *emf* in aqueous solutions and normality–inertia parameter of some electrodeposited metals.

Reaction	$\Delta h_{\text{ion}}^\circ/zF$	$(\Delta h_{\text{ion}}^\circ + \Delta h_{\text{hydr}}^\circ)/zF$	$\Delta h_{\text{cell}}^\circ/zF$	E°/V	P_{NI}
$H_2 = 2H^+ + 2e^-$	13.6626	2.3551	4.6142	0.0000	1.000
$Fe = Fe^{2+} + 2e^-$	12.1050	1.9775	4.1349	-0.47	0.945
$Co = Co^{2+} + 2e^-$	12.5222	2.0547	4.2727	-0.277	0.973
$Ni = Ni^{2+} + 2e^-$	12.9909	2.0794	4.2825	-0.257	0.999
$Cu = Cu^{2+} + 2e^-$	14.093	3.0236	4.9552	0.34	0.863
$Pd = Pd^{2+} + 2e^-$	13.9462	3.4265	5.3863	0.915	0.819
$Zn = Zn^{2+} + 2e^-$	13.5408	3.1447	3.8222	-0.763	0.615
$Pb = Pb^{2+} + 2e^-$	11.287	3.618	4.623	-0.126	0.539
$Pt = Pt^{2+} + 2e^-$	13.6488	2.823	5.7522	1.188	1.039

The electrochemical behavior of the elements in aqueous solutions, i.e., the kinetics of ionic exchange, depends primarily on the bonding state of the chemical species in the intervening phases, the crystal lattice and the aqueous solution. In other words, it can be related to the relative value of the different enthalpy changes involved in the process, as described above. The definition of a parameter expressing the degree of electrochemical inertia (or reversibility) can be attempted based on the relative weight of the different enthalpy terms involved in the process. The proposed procedure consists in

weighting the value of the ionization enthalpy to the enthalpy change for the hydration of the gaseous atom and normalizing this ratio to the enthalpy change of the overall process. In fact, the ionization term refers specifically to the elementary step of charge transfer through the interface—the fundamental physical process in the electrochemical reaction—and reflects the role of the electronic structure as a dominant factor determining the electrochemical inertia of the elements, while the hydration enthalpy has a counteracting action in the energetics of the process, referring to the strength of the bonding in the electrolyte phase. Therefore, by the ratio of the enthalpy change for the ionization reaction $\Delta h_{\text{ion}}^{\circ}$ to the enthalpy change for the hydration of the gaseous atom $\Delta h_{\text{ion}}^{\circ} + \Delta h_{\text{hydr}}^{\circ}$ and with respect to the whole enthalpy change $\Delta h_{\text{at}}^{\circ} + \Delta h_{\text{ion}}^{\circ} + \Delta h_{\text{hydr}}^{\circ}$, an electrochemical electronegativity R_{NI} is defined for the element M, through the relation

$$R_{\text{NI}} = \Delta h_{\text{ion}}^{\circ} / (\Delta h_{\text{ion}}^{\circ} + \Delta h_{\text{hydr}}^{\circ}) / (\Delta h_{\text{ion}}^{\circ} + \Delta h_{\text{hydr}}^{\circ} + \Delta h_{\text{at}}^{\circ}) \quad (4)$$

Comparing R_{NI} with the electrochemical electronegativity of hydrogen (as normal in aqueous solution) the *normality–inertia parameter* P_{NI} results:

$$P_{\text{NI}} = \frac{\left[\Delta h_{\text{ion}}^{\circ} / (\Delta h_{\text{ion}}^{\circ} + \Delta h_{\text{hydr}}^{\circ}) / (\Delta h_{\text{ion}}^{\circ} + \Delta h_{\text{hydr}}^{\circ} + \Delta h_{\text{at}}^{\circ}) \right]_{\text{M}}}{\left[\Delta h_{\text{ion}}^{\circ} / (\Delta h_{\text{ion}}^{\circ} + \Delta h_{\text{hydr}}^{\circ}) / (\Delta h_{\text{ion}}^{\circ} + \Delta h_{\text{hydr}}^{\circ} + \Delta h_{\text{at}}^{\circ}) \right]_{\text{H}}} \quad (5)$$

Figures 1A,B show a linear relation between the logarithm of i_{M}° or i_{H}° and P_{NI} obtained from literature results.

Table 1 reports the values of the different enthalpic contributions, the cell voltage, and the normality–inertia parameter P_{NI} for typical inert (Fe, Co, Ni), intermediate (Cu, Pd) and normal metals (Pb, Zn) in simple solutions. With the parameter P_{NI} , it is also possible to distinguish among the different electrokinetic behavior of similar metals. In this respect, the case of the anomalous codeposition is enlightening; Fe is discharged first in a solution containing Co or Ni; analogously, Co is discharged before Ni. This so-called anomalous behavior is readily justified by the value of the P_{NI} parameter for these elements (see Table 1), pointing to the decisive role of ion–water interaction in determining the relative inertia in the ionic exchange process of the Fe group metals. Notably, the anomalous character of the deposition is reduced in the presence of complexing agent, e.g., the Ni/Fe mass ratio is drastically increased in deposit from electrolyte containing ethylenediamine [58]. In some cases, metals can have P_{NI} greater than one (e.g., Pt), when H is discharged first and we must introduce complexants to discharge the metal ion, in order to passivate the surface with respect to H exchange.

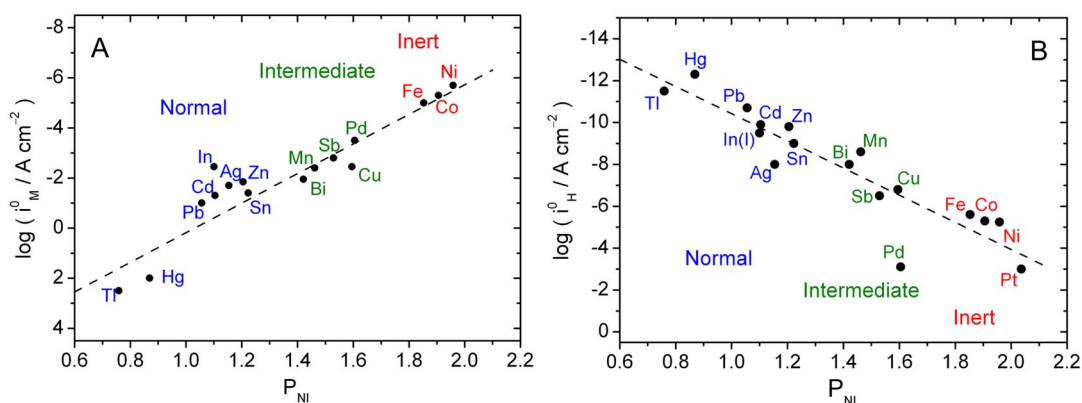


Fig. 1 Dependence on P_{Ni} on $\log i_M^0$ for electrodeposited metals (A) and $\log i_H^0$ for H_2 evolution on the same metals (B).

EXPERIMENTAL DETAILS

All the electrochemical experiments were performed in prismatic pyrex cells with about 300 ml of solution. The plating solutions were prepared from analytical grade chemicals and distilled water.

The electrochemical measurements were performed in a three-electrode configuration utilizing a measuring cell with either an Ag/AgCl reference electrode RE in connection to the working electrode WE with a lateral-channel Piontelli probe (mean distance of the lateral slit from the surface 30 μm [59]) or—for transient measurements—a platinum mesh as pseudo-reference electrode. The later electrode was preliminarily checked in the electrolyte under study for reproducibility and stability, and found to be always reliable for measurements on the time span of the transients. All the electrodeposition experiments were performed on Cu cathodes coated with amorphous Ni-P (P 9 %) deposited from a chemical autocatalytic bath described elsewhere [60].

The phase structure and the texture of the deposits were investigated by X-ray diffractometry with $\text{CuK}\alpha$ radiation and a powder goniometer. The operating conditions (accelerating voltage, electron beam current, and angular scanning rate) were chosen in order to achieve signal to noise ratios in excess of 5.5 over the peaks of interest [61].

The surface morphology of the deposits was investigated by scanning electron microscopy (SEM), the dimension of surface features was estimated with image analysis software [62].

MODELING: SECONDARY CURRENT PULSE TECHNIQUE

Electrokinetic parameters were obtained by us with the secondary current pulse (SCP) technique [64–66], where a short square galvanostatic pulse of a few ms is superimposed on the cathode while electrodeposition is running. The increase of cd $\Delta i = i_P - i_D$ (where i_P and i_D are the pulse and deposition, cd, respectively) is attributed to a capacitive i_C and a faradaic i_F term, i.e., $i = i_C + i_F$, according to the following expressions

$$i_C = C_{\text{ads}} \cdot \exp\left(\frac{\eta}{B_T}\right) \cdot \frac{d\eta}{dt}; i_F = i_D \cdot \exp\left(\frac{\eta}{B_T}\right) \quad (6)$$

where both components of the cd are assumed to depend exponentially on the overvoltage η , noting that the exponential dependence of the capacitive cd on overvoltage was underlined by Heusler in his work on cobalt electrocrystallization [63].

As shown by eqs. 6 and 7, two parameters are obtained from the transient overvoltage increase: the adsorption pseudo-capacitance C_{ads} , determining the starting $\eta(t)$ slope and the transient Tafel slope B_T , determining the asymptotic $\eta(t)$ value. The following expression ensues from the assumptions made:

$$\eta = B_T \cdot \ln \left[\frac{i_P}{i_D} - \frac{i_P - i_D}{i_D} \cdot \exp \left(- \frac{i_D \cdot t}{B_T \cdot C_{\text{ads}}} \right) \right] \quad (7)$$

In some cases, a pseudo-diffusion term must be added to $\eta(t)$, related to the possible composition changes in the layer adjoining the surface [64–67]

$$\eta_D(t) = \frac{RT}{zF} \cdot \sqrt{\frac{t}{\tau}} \quad (8)$$

with the assumption that the pseudo-diffusion follows a Sand-type behavior with a transition time constant τ . The transition time constant is accordingly related to the concentration of the reacting species C_S and its diffusion coefficient D through the relation: $i\tau^{1/2} = zFC_S(\pi D/4)^{1/2}$, from which the constant parameter $C_S D^{1/2} = i\tau^{1/2}/(\pi^{1/2} F)$ is derived.

These parameters can be related to the growth of the metal electrodeposited and are of particular importance for the control of nano electrodeposition, in particular for magnetic and wear-resistant layers [67].

B_T is related to the steady-state value reached after the charging transient, observed if no diffusion phenomena are present; otherwise, it can be inferred from the time behavior of the transient, which in that case depends upon two time constants, associated with the pseudo-capacitive faradaic process and the diffusion-like process.

The transient capacitive behavior of the electrode is related to the faradaic effect, depending on the nature and amount of electroactive species adsorbed at the electrode. $C_{\text{ads}}(\eta) = C_{\text{ads}} \cdot \exp(\eta/B_T)$ describes the electroodic capacitive behavior related to faradaic phenomena. C_{ads} is markedly affected by hydrolytic phenomena: the precipitation of hydroxides and basic salts in the bath corresponds to values of C_{ads} up to 1 mF cm⁻², while $C_{\text{ads}} < 100 \mu\text{F cm}^{-2}$ if hydrolyzed species are stable only at the electroodic surface.

The observed values of the parameter τ were typically in the range of 10 ms and are obviously unrelated with the convective transport conditions established in our cells. Our experimental values of τ can be explained if we consider a progressive lowering of the surface concentration of the reactant, not because the Nernst layer is depleted when electrodeposition is fast and diffusion of metallic cations from the bulk is slow, but because the cathodically formed (in steady state) electroactive intermediates are consumed by electrodeposition reactions and diffusion from the inner Helmholtz layer into the Nernst diffusion layer and the bulk.

RESULTS

Copper electrokinetic behavior

The influence of complexants on the electrokinetic behavior and the normality–inertia parameter of metals can be well shown in the case of copper deposition from different solutions.

Complexants decrease the standard cell voltage and increase P_{Ni} . The latter effect is readily explained considering that complexation basically involves a stabilization of the ionic state, i.e., the increase of the strength of ionic bonding in the electrolyte phase, contributing to the electrochemical inertia of discharging species in the cathodic reduction. The same effect appears on the anodic side with the difference that the inertia here is due to surface passivation engendered by strong ion–ligand interaction.

When the complexation constant is very high, the P_{NI} value becomes greater than one. In this case, different discharge reactions at the cathode, involving the complex species, must be considered, with electrons directly reacting with the complex ion. Table 2 reports the case of copper from simple solutions and from solutions with pyrophosphate and cyanide ligands.

Table 2 Standard emf in aqueous solutions and normality–inertia parameter for copper electrodeposited from different solutions.

Reaction	$\Delta h^\circ_{\text{ion}}/zF$	$(\Delta h^\circ_{\text{ion}} + \Delta h^\circ_{\text{hydr}})/zF$	$\Delta h^\circ_{\text{cell}}/zF$	E°/N	P_{NI}
$\text{Cu} = \text{Cu}^{2+} + 2e^-$	14.093	3.204	4.9552	0.34	0.814
$\text{Cu} + \text{P}_2\text{O}_7^{4-} = \text{Cu}(\text{P}_2\text{O}_7)^{2-} + 2e^-$	14.093	3.004	4.7552	0.14	0.834
$\text{Cu} = \text{Cu}^+ + e^-$	7.801	1.8583	5.3614	0.52	0.841
$\text{Cu} + 2\text{CN}^- = \text{Cu}(\text{CN})_2^- + e^-$	7.801	0.8983	4.4014	-0.44	1.428

Results are presented in Fig. 2 top for copper electrodeposited from CuSO_4 1 M, H_2SO_4 0.5 M solution, room T, 10 mA cm^{-2} , after 1 h on a Cu sheet plated with NiP ACD, the preferred orientation PO is a small [100], the transient SCP parameters are $B_{\text{T}} 95 \text{ mV dec}^{-1}$, $C_{\text{ads}} 20 \mu\text{F cm}^{-2}$, $\tau 20 \text{ ms}$.

Figure 2 bottom refers to copper electrodeposited from $\text{Cu}_2\text{P}_2\text{O}_7$ 0.25M, $\text{K}_4\text{P}_2\text{O}_7$ 1 M solution, pH 8.75, 30°C , 10 mA cm^{-2} after 1 h on a similar substrate; a strong [110] PO is obtained, the transient SCP parameters become $B_{\text{T}} 230 \text{ mV dec}^{-1}$, $C_{\text{ads}} 96 \mu\text{F cm}^{-2}$, $\tau 3 \text{ ms}$.

This example shows the typical great increase of the transient Tafel slope parameter (almost $4RT/F$), that is related to the asymptotic overvoltage, in the solution with a strong complexant.

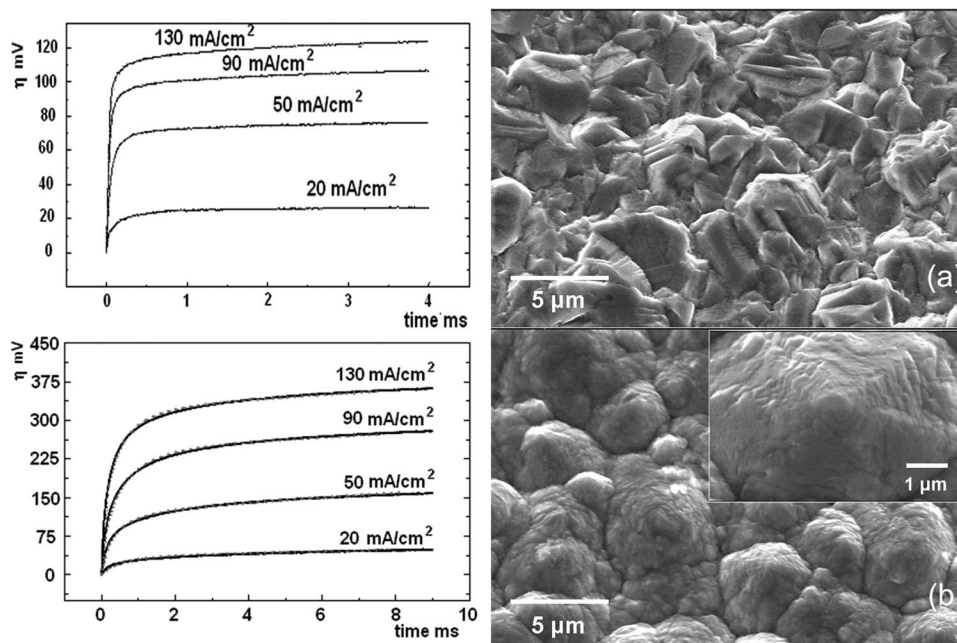


Fig. 2 (a) SCP on Cu deposited from CuSO_4 1 M, H_2SO_4 0.5 M, room T, 10 mA cm^{-2} , pulse current 20, 50, 90, or 130 mA cm^{-2} ; SEM micrograph of Cu deposit after 1 h with a faint [100] PO. (b) SCP on Cu deposited from $\text{Cu}_2\text{P}_2\text{O}_7$ 0.25 M, $\text{K}_4\text{P}_2\text{O}_7$ 1 M, pH 8.75, 30°C , 10 mA cm^{-2} , pulse current 20, 50, 90, or 130 mA cm^{-2} ; SEM micrograph of Cu deposit after 1 h, with [110] PO.

Cobalt cellular electrodeposition

Cobalt deposition is of great interest for its magnetic applications, but also for wear resistance. Cobalt is an HCP metal and can be deposited with basal plane parallel to the substrate; in this case, for the lowest friction coefficient is obtained on the $\{00.1\}$ preferred slip planes [68], optimal wear performance can be achieved.

Cobalt can be electrodeposited with different well-defined preferred orientations according to the deposition conditions [65]. Deposition of the iron group metals from sulfamate solutions is particularly interesting, permitting a better control of hydroxides and basic salts precipitation compared to traditional sulfate or sulfate–chloride-based baths, as it is well known in the case of electrodeposited nickel.

We have deposited cobalt from a $\text{Co}(\text{NH}_2\text{SO}_3)_2$ 1 M, H_3BO_3 0.5 M solution, pH 4 to 4.8, 30 °C, 10 mA cm^{-2} ; in this case, typical ridges $4 \mu\text{m}$ long are observed, as shown in Fig. 3a. The preferred orientation is a quite strong $[10.0] + [11.0]$ PO (the two PO are related and are present on the two opposite sides of the ridge [21]). From SCP measurements, the following parameters are obtained: B_T 160 mV dec^{-1} , C_{ads} $60 \mu\text{F cm}^{-2}$. The very high value of B_T can be related to the complexing action of the boric acid with respect to cobalt ions [65].

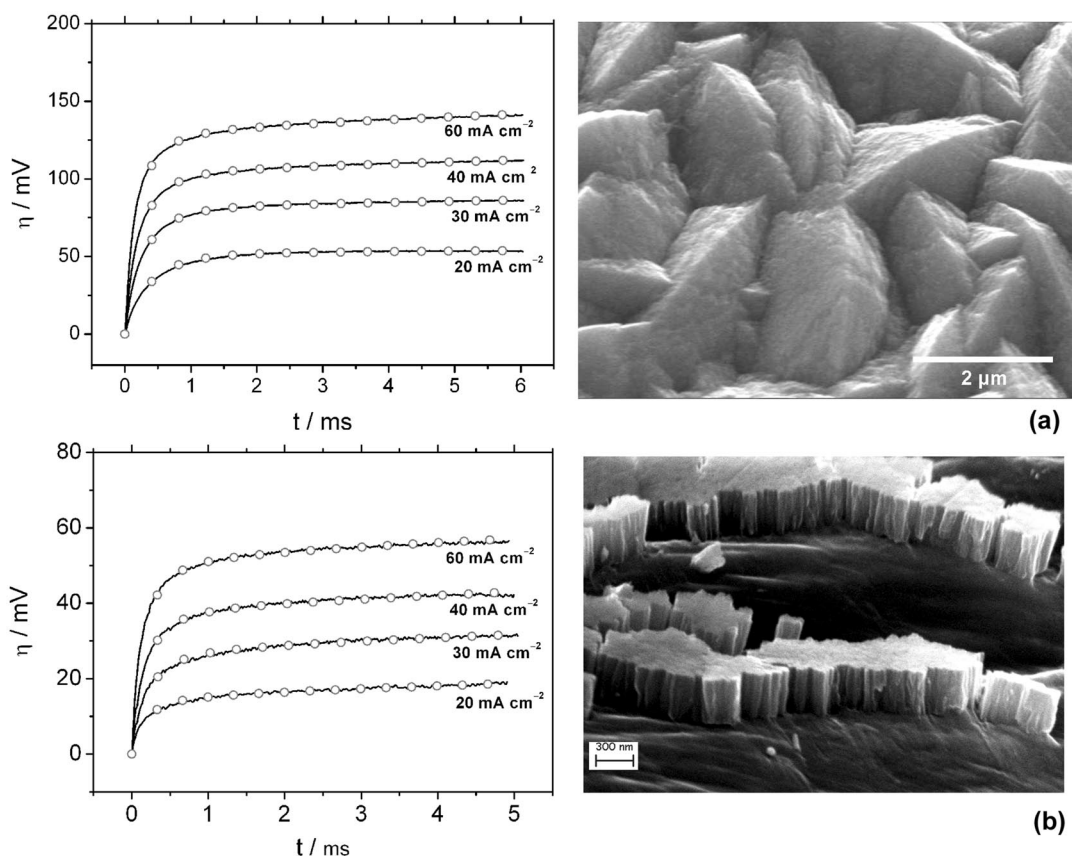


Fig. 3 (a) SCP on Co deposited from $\text{Co}(\text{NH}_2\text{SO}_3)_2$ 1 M, H_3BO_3 0.5 M, pH 4.8, room T, 10 mA cm^{-2} , pulse current 20, 30, 40, or 60 mA cm^{-2} ; SEM micrograph on Co deposit after 1 h, with $[11.0] + [10.0]$ PO. (b) SCP on Co deposited from $\text{Co}(\text{NH}_2\text{SO}_3)_2$ 1 M, $\text{H}_4\text{N}_2\text{O}_2\text{S}$ 5 mM, pH 6.0, room T, 10 mA cm^{-2} , pulse current 20, 30, 40, or 60 mA cm^{-2} ; SEM micrograph of Co deposit after 3 min, with very strong $[00.1]$ PO.

A peculiar structure can be deposited from a solution containing $\text{Co}(\text{NH}_2\text{SO}_3)_2$ 1 M and $\text{H}_4\text{N}_2\text{O}_2\text{S}$ 5 mM, operating at pH 6, 30 °C, and 10 mA cm^{-2} . The preferred orientation is a very strong [00.1] PO, cobalt has a fibrous structure, with almost single-crystalline columns, separated from hydroxide or basic salt precipitation, as shown in Fig. 3b. This type of growth is interpreted as a *cellular growth*, because, at variance with the ordinary columnar growth obtained either in vapor-deposited or in electrodeposited films, it is uniquely characterized by the strong texture and the attendant grain boundary structure, in other words, for being a grain boundary engineered material. It is obtained in conditions of strong inhibition at the surface, when hydrolyzed species are stable into the bulk of the bath and can precipitate as basic salts at the grain boundary. From SCP measurements, the following parameters are obtained: B_T 50 mV dec^{-1} , C_{ads} 120 $\mu\text{F cm}^{-2}$. The low value of B_T ($< RT/F$) can be related to the occupation of the surface by the hydrolyzed species, from which cobalt can be discharged, correspondingly, the C_{ads} is very high.

This type of growth can be regarded as intermediate between normal and dendritic growth. Figure 4 shows a cellular growth of cobalt on the substrate, with single cobalt columns, and a dendritic growth following, obtained, after interruption, by cobalt deposition at much higher current density.

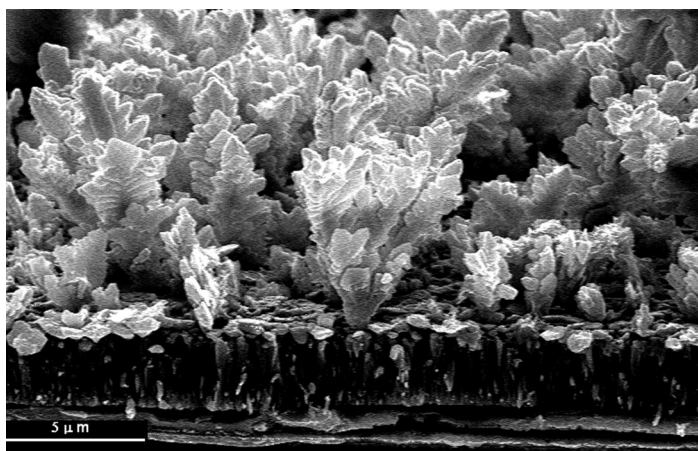


Fig. 4 SEM micrograph of Co deposited from $\text{Co}(\text{NH}_2\text{SO}_3)_2$ 1 M, pH 6.0, room T showing the transition from cellular to dendritic growth.

The obtainment of cellular growth can be related to the development of a morphological instability during electrodeposition. Many authors, starting from the work of Mullins and Sekerka [69–71] on the stability during the solidification of a dilute binary alloy, have developed a theoretical approach for the interpretation of powder formation during electrodeposition [72,73] and of roughness evolution in electrochemical processes with possible formation of dendrites [74]. The fundamental equation to interpret the instability formation at a surface during electrodeposition is, according to Barkey et al. [75,76]

$$\frac{\partial \ln H}{\partial \tau} = \frac{F_c + F_e - F_s}{1 + W_c + W_a} \quad (9)$$

where H is the amplitude of the perturbation mode; $\tau = t \frac{k_s v RT}{(zF\delta)^2}$ an adimensional time; $F_e = \frac{zF\delta}{k_s RT} i$

the electrostatic field; $F_c = \frac{i/i_L}{1 - i/i_L}$ the concentration field; $F_s = \frac{\delta \kappa v \gamma}{RT}$ the surface excess free energy

term; $W_c = \frac{RTk_s}{zF\delta(1-i/i_L)i_L}$ the concentration Wagner number; and $W_a = \frac{RTk_s}{i\beta_c zF\delta}$ the activation Wagner number.

In these expressions, k_s is the solution conductivity, v the molar volume of the electrodeposited metal, δ the Nernst diffusion layer thickness; i_L the limiting current density, k the surface curvature, γ the surface excess free energy, β_c the Tafel slope.

$$\text{If } i \ll i_L: F_c \cong \frac{i}{i_L} \text{ and } W_c = \frac{RTk_s}{zF\delta \cdot i_L}$$

Introducing a surface profile: $y = H \sin \omega x$, with $\omega = 2\pi/\lambda$ the sign of $\partial \ln H / \partial t$ will depend on the sign of: $\frac{i}{k_s} - \frac{\kappa \gamma v}{zF}$ with $\kappa = 2 \omega^2$.

The values for Co in its solution are: $v = 7 \cdot 10^{-6} \text{ m}^3 \text{ mol}^{-1}$; $\gamma = 0.3 \text{ J m}^{-2}$; $z = 2$; $F = 10^5 \text{ C eq}^{-1}$; $k_s = 1 \text{ } \Omega^{-1} \text{ cm}^{-1}$ and assuming $i = 100 \text{ A m}^{-2}$ we obtain

$$\lambda = 2\pi \left(\frac{2v\gamma k_s}{izF} \right)^{1/2} = 6.28 \left(\frac{2 \cdot 7 \cdot 10^{-6} \cdot 0.3 \cdot 1}{100 \cdot 2 \cdot 10^5} \right)^{1/2} = 2.9 \cdot 10^{-6} \text{ m} = 2.9 \text{ } \mu\text{m}$$

Reasonably, the strong surface inhibition can decrease the conductivity in the adsorbed layer to very low values such as $k_s = 0.01 \text{ } \Omega^{-1} \text{ cm}^{-1}$ as well as induce a reduction in the surface tension, e.g., to 0.15 J m^{-2} , in this case, we obtain a value of

$$\lambda = 6.28 \left(\frac{2 \cdot 7 \cdot 10^{-6} \cdot 0.15 \cdot 0.01}{100 \cdot 2 \cdot 10^5} \right)^{1/2} = 2 \cdot 10^{-7} \text{ m} = 0.2 \text{ } \mu\text{m}$$

which is much closer to the actual observed value.

Surface definition is crucial for further developments, such as dry lubrication, in this case a solid lubricant, that can be a soft metal or a fluorine polymer, can be deposited or adsorbed between the columns, assuring a great decrease of the friction coefficient and a strong increase of the wear resistance.

Ni–Co alloy electroforming

For many applications of electroformed parts, it is important to increase the mechanical properties of the deposited metals. Nickel electroforming is normally employed for these applications, to increase its hardness a possible simple solution is to add cobalt in the bath, thus depositing a Ni–Co alloy. We have studied this addition to a typical Ni sulfamate bath for electroforming, obtaining in special conditions deposits with very low internal stresses in the order of less than 0.1 MPa.

The electrokinetic SCP behavior of a bath that was operated for some years is presented here. The bath contained $\text{Ni}(\text{SO}_3\text{NH}_2)_2$ 2 M, H_3BO_3 0.5 M, sodium dodecyl sulfate 1.7×10^{-3} M. It was operating at 50 °C and pH 4. The deposited Ni showed a relatively strong (110) PO, and the deposit hardness was about 250 HV.

Adding to the bath $\text{Co}(\text{SO}_3\text{NH}_2)_2$ 8×10^{-3} M, it was possible to obtain at 10 mA cm^{-2} a Ni–Co alloy deposit containing about Co 21 wt %, with a hardness of $470 \pm 10 \text{ HV}$ (200 mN load). The structure was very fine grained, as shown in Fig. 5, the crystallographic structure showed a faint (110) PO, the crystal size, determined by the Williamson–Hall method, was in the range of 20 nm compared to about 50 nm for the pure nickel deposit, which in addition shows a much coarser grain structure.

Transient parameters, from the SCP measurements shown in Fig. 5, had the following values:
 for Ni: B_T 110 mV dec⁻¹, C_{ads} 47 μ F cm⁻², $C_b D^{1/2}$ 22 nM cm⁻²s⁻¹
 for Ni-Co: B_T 105 mV dec⁻¹, C_{ads} 45 μ F cm⁻², $C_b D^{1/2}$ 37 nM cm⁻²s⁻¹

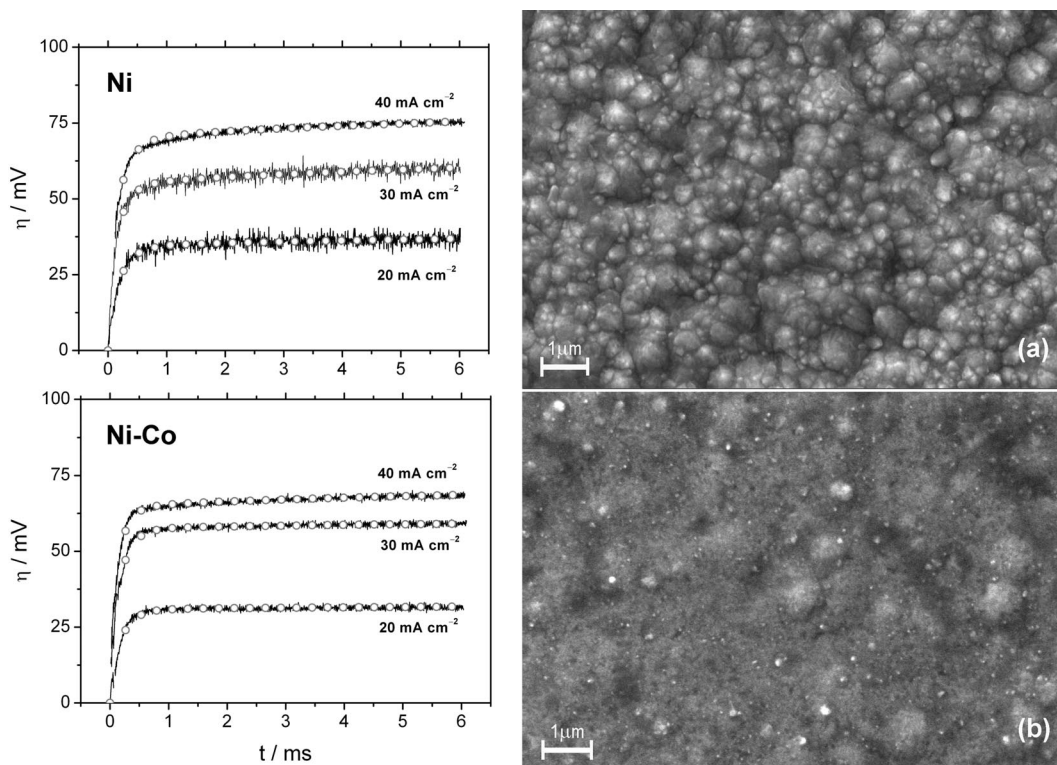


Fig. 5 (a) SCP on Ni deposited from $\text{Ni}(\text{NH}_2\text{SO}_3)_2$ 2 M, H_3BO_3 0.5 M, pH 4.0, 50 °C, 10 mA cm⁻², pulse current 20, 30, or 40 mA cm⁻²; SEM micrograph on Ni deposit after 1 h, with [110] PO. (b) SCP on Ni-Co deposited from same bath with addition of $\text{Co}(\text{NH}_2\text{SO}_3)_2$ 8×10^{-3} M, pH 4.0, 50 °C, 10 mA cm⁻², pulse current 20, 30, or 40 mA cm⁻²; SEM micrograph of Ni-Co 21 % deposit after 1 h, with a faint [110] PO.

As shown by the SCP results, the discharge kinetics is only slightly affected, in connection with a seemingly activating effect of cobalt ions determined by the anomalous codeposition behavior, resulting in both slightly lower B_T and C_{ads} values. The main effect is on the pseudo-diffusive behavior during the transient, which reflects the changes in the dynamic interaction between the different species present at the surface and in the near surface region. The weaker interaction of the Co ions with water, compared with that of the Ni ions—as shown by the P_{Ni} parameter—translates into a relatively faster rate of formation of discharge intermediates by the direct interaction of Co aqua-ions and back-diffusing oxy-hydrates, resulting in a smaller polarization effect during the transient.

CONCLUSIONS

The structure of electrodeposited metals depends strongly on the electrodeposited metal and on the electrolytic solution, especially if a complex bath is adopted, as well as on the deposition operative conditions.

A strong relation exists between the electrokinetic parameters and the preferred orientation developed. The parameter of normality–inertia P_{NI} is a parameter describing the electrokinetic behavior of the bath and permitting an electrokinetic classification of the electrodeposited metal.

With the SCP method it is possible to obtain three electrokinetic parameters: the adsorption pseudo-capacitance C_{ads} (related to the adsorption of the discharging species at the surface), the transient Tafel slope B_T (related to the asymptotic value of the transient activation overvoltage), and the time constant τ (related to the relaxation of the surface concentration of the discharging species). The SCP method being a transient technique with very limited influence on the deposit growth, these parameters describe the real electrokinetic behavior at the surface during electrodeposition.

We have reported about the electrokinetic behavior of copper baths and its relation to the structure of deposited copper showing the strong influence of the ligand controlling the growth.

The case of cobalt cellular electrodeposition was introduced to show the possibility of controlling the structure at the nanolevel through strong inhibition. In this case, lateral growth prevails, with respect to the more usual outgrowth or cluster growth. Cellular growth occurs in intermediate conditions between normal and dendritic growth. It was observed for cobalt, cobalt–platinum, copper, zinc, and gold. Immediate application regards dry lubrication and hard magnetic features.

The sulfamate electrolyte developed for Ni–Co electroforming gives nanocrystalline deposits with grain size about 20 nm and increased hardness, even at low cd. Alloying in electrodeposition is a straightforward route toward the production of nanocrystalline materials; particularly, as in the case here examined, in conditions of slightly faster activation kinetics coupled to enhanced nucleation.

REFERENCES

1. G. Finch, A. Quarrel, H. Wilman. *Trans. Faraday Soc.* **31**, 1051 (1935).
2. G. Finch, C. Sun. *Trans. Faraday Soc.* **32**, 852 (1936).
3. G. Finch, A. Williams. *Trans. Faraday Soc.* **33**, 564 (1937).
4. G. Finch, L. Yang. *Discuss. Faraday Soc.* **1**, 144 (1947).
5. G. Finch. *Z. Elektrochem.* **54**, 457 (1950).
6. G. Finch, D. Layton. *J. Electrodepositors' Tech. Soc.* **27**, 215 (1951).
7. H. Fischer. *Elektrolytische Abscheidung und Elektrokristallisation von Metallen*, Springer, Berlin (1954).
8. H. Fischer. *Electrochim. Acta* **2**, 50 (1960).
9. G. Eichkorn, F. W. Schlitter, H. Fischer. *Z. Phys. Chem.* **62**, 1 (1968).
10. H. Fischer. *Angew. Chem., Int. Ed.* **8**, 108 (1969).
11. H. Fischer. *Plating* **56**, 1229 (1969).
12. (a) H. Fischer. *Electrodepos. Surf. Treat.* **1**, 239 (1972/73); (b) H. Fischer. *Electrodepos. Surf. Treat.* **2**, 319 (1972/73).
13. R. Winand. *Hydrometallurgy* **29**, 567 (1992).
14. N. A. Pangarov. *J. Electroanal. Chem.* **9**, 70 (1965).
15. N. A. Pangarov. *Electrochim. Acta* **9**, 721 (1964).
16. N. A. Pangarov, S. D. Vitkova. *Electrochim. Acta* **11**, 1733 (1966).
17. A. Reddy. *J. Electroanal. Chem.* **6**, 141 (1963).
18. (a) A. Reddy, S. Ragopalayan. *J. Electroanal. Chem.* **6**, 153 (1963); (b) A. Reddy, S. Ragopalayan. *J. Electroanal. Chem.* **6**, 159 (1963).
19. M. Froment. *J. Microscopie* **3**, 61 (1964).
20. M. Froment, G. Maurin. *J. Microscopie* **7**, 39 (1968).
21. I. Epelboin, M. Froment, G. Maurin. *Plating* **56**, 1356 (1969).
22. J. Amblard, M. Froment, N. Spyrellis. *Surf. Technol.* **5**, 205 (1977).
23. J. Amblard, M. Froment. *Discuss. Faraday Soc.* **12**, 126 (1978).
24. J. Amblard, I. Epelboin, M. Froment, G. Maurin. *J. Appl. Electrochem.* **9**, 233 (1979).

25. N. Spyrellis, J. Amblard, G. Maurin. *Oberflaeche-Surf.* **11**, 458 (1985).
26. N. Spyrellis, J. Amblard, M. Froment, G. Maurin. *J. Microsc. Spectrosc. Electron.* **12**, 220 (1987).
27. M. Froment, G. Maurin. *J. Microsc. Spectrosc. Electron.* **12**, 379 (1987).
28. C. Kollia, N. Spyrellis, J. Amblard, M. Froment, G. Maurin. *J. Appl. Electrochem.* **20**, 1025 (1990).
29. C. Kollia, N. Spyrellis. *Surf. Coat. Technol.* **57**, 71 (1993).
30. F. Kotzia, C. Kollia, N. Spyrellis. *Trans. Inst. Met. Finish.* **71**, 34 (1993).
31. C. Kollia, N. Spyrellis. *Trans. Inst. Met. Finish.* **72**, 124 (1994).
32. I. Macheras, D. Vouros, C. Kollia, N. Spyrellis. *Trans. Inst. Met. Finish.* **74**, 55 (1996).
33. E. A. Pavlatou, M. Raptakis, N. Spyrellis. *Surf. Coat. Technol.* **201**, 4571 (2007).
34. A. Pavlatou, N. Spyrellis. *Russ. J. Electrochem.* **44**, 745 (2008).
35. E. Budevski, G. Staikov, W. J. Lorenz. *Electrochemical Phase Formation and Growth*, VCH, Weinheim (1996).
36. J.-P. Celis, P. Cavallotti, J. Machado Da Silva, A. Zielonka. *Trans. Inst. Met. Finish.* **76**, 163 (1998).
37. W. Ruythooren, K. Attenborough, S. Beerten, P. Merken, J. Fransaeer, E. Beyne, C. Van Hoof, J. De Boeck, J. P. Celis. *J. Micromech. Microeng.* **10**, 101 (2000).
38. P. C. Andricacos, C. Uzoh, J. O. Dukovic, J. Horkans, H. Deligianni. *IBM J. Res. Dev.* **42**, 567 (1998).
39. A. Milchev. *Electrocrystallization Fundamentals of Nucleation and Growth*, 1st ed., Kluwer Academic, Boston (2002).
40. D. Y. Li, J. A. Szpunar. *Electrochim. Acta* **42**, 37 (1997).
41. J. Liu, C. Liu, P. P. Conway. *Electrochim. Acta* **54**, 6941 (2009).
42. G. Staikov (Ed.). *Electrocrystallization in Nanotechnology*, John Wiley, New York (2007).
43. R. Piontelli. *J. Chim. Phys.* **46**, 288 (1949).
44. R. Piontelli. *Z. Elektrochem.* **55**, 128 (1951).
45. (a) R. Piontelli. *Proc. II CITCE*, p. 163, Tamburini, Milano (1951); (b) R. Piontelli. *Proc. III CITCE*, Manfredi, Milano (1951).
46. T. Erdey-Gruz. *Kinetics of Electrode Processes*, A. Hilger Ltd., London (1972).
47. R. Piontelli, G. Poli, G. Serravalle. In *Trans. Symp. on Electrode Processes*, E. Yeager (Ed.), p. 67, John Wiley, New York (1959).
48. R. Piontelli. *Electrochim. Metall.* **1**, 5 (1966).
49. P. L. Cavallotti, D. Colombo, U. Ducati, A. Piotti. In *Electrodeposition Technology Theory and Practice*, L. Romankiw, D. A. Turner (Eds.), ECS Proc. 87-17, p. 429, ECS Pub., Pennington (1987).
50. P. L. Cavallotti, B. Bozzini, L. Nobili, G. Zangari. *Electrochim. Acta* **39**, 1123 (1994).
51. J. A. V. Butler. *Electrocapillarity*, Chemical Publishing, New York (1940).
52. S. Trasatti. *Pure Appl. Chem.* **58**, 955 (1986).
53. H. F. Halliwell, S. C. Nyburg. *Trans. Faraday Soc.* **59**, 1126 (1963).
54. W. E. Dasent. *Inorganic Energetics*, Cambridge University Press, Cambridge, UK (1982).
55. W. M. Latimer. *Oxidation Potentials*, 2nd ed., Prentice Hall, Englewood Cliffs (1952).
56. A. J. Bard, R. Parsons, J. Jordan. *Standard Potentials in Aqueous Solutions*, Marcel Dekker, New York (1985).
57. A. J. de Bethune, T. S. Licht, N. A. Swendeman. *J. Electrochem. Soc.* **106**, 616 (1959).
58. T. M. Harris, J. St. Clair. *J. Electrochem. Soc.* **143**, 3918 (1996).
59. R. Piontelli, G. Serravalle, G. Poli. *Rend. Acc. Naz. Lincei, Serie VIII* **25**, 431 (1958).
60. B. Bozzini, P. Cavallotti, M. V. Ivanov, A. Buratti, F. Krüger. *Proc. Interfinish 1992*, p. 156, São Paulo (1992).
61. M. F. Koenig, J. T. Grant. *Surf. Interf. Anal.* **7**, 217 (1985).

62. B. Bozzini, P. L. Cavallotti, G. Giovannelli, B. Brevaglieri, S. Natali. *Prakt. Metallogr.* **33**, 130 (1996).
63. K. E. Heusler. *Ber. Bunsenges. Phys. Chem.* **71**, 620 (1967).
64. A. Vicenzo, P. L. Cavallotti. *J. Appl. Electrochem.* **32**, 743 (2002).
65. A. Vicenzo, P. L. Cavallotti. *Electrochim. Acta* **49**, 4079 (2004).
66. A. Vicenzo, P. L. Cavallotti. *Russ. J. Electrochem.* **44**, 716 (2008).
67. P. L. Cavallotti, M. Bestetti, S. Franz, A. Vicenzo. *Trans. Inst. Met. Finish.* **88**, 178 (2010).
68. D. H. Buckley, R. L. Johnson. *Wear* **11**, 405 (1968).
69. (a) W. Mullins, R. F. Sekerka. *J. Appl. Phys.* **34**, 323 (1963); (b) W. Mullins, R. F. Sekerka. *J. Appl. Phys.* **35**, 444 (1964).
70. R. F. Sekerka. *J. Appl. Phys.* **36**, 264 (1965).
71. R. F. Sekerka. *J. Phys. Chem. Solids* **28**, 983 (1967).
72. R. Aogaki, K. Kitazawa, Y. Kose, K. Fueki. *Electrochim. Acta* **25**, 965 (1980).
73. R. Aogaki, T. Makino. *Electrochim. Acta* **26**, 1509 (1981).
74. U. Landau, J. H. Shyu. *EPRI Report EM-2937*, Palo Alto, CA (1983).
75. (a) D. P. Barkey, R. H. Muller, C. W. Tobias. *J. Electrochem. Soc.* **136**, 2199 (1989); (b) D. P. Barkey, R. H. Muller, C. W. Tobias. *J. Electrochem. Soc.* **136**, 2207 (1989).
76. D. P. Barkey. In *Advances Electrochemical Science and Engineering* 7, R. C. Alkire, D. M. Kolb (Eds.), pp. 151–191, Wiley-VCH, Weinheim (2002).